A REVIEW ON THE BOND BEHAVIOR OF FRP NSM SYSTEMS IN CONCRETE

Mário R. F. Coelho[1,2], José M. Sena-Cruz[1,3], Luís A. C. Neves[4,5]

[1] ISISE, University of Minho, Department of Civil Engineering, Campus de Azurém, 4810-058 Guimarães, Portugal

[2] E-mail: mcoelho@civil.uminho.pt; *Corresponding author*

[3] E-mail: jsena@civil.uminho.pt

[4] University of Nottingham, Department of Civil Engineering, Nottingham, United Kingdom

[5] E-mail: luis.neves@nottingham.ac.uk

Abstract: This paper presents a review of current knowledge on the bond behavior of fiber reinforced polymer (FRP) systems inserted in the cover of concrete elements, commonly known as the near-surface mounted technique (NSM). In the first part, by studying the physics of the phenomenon, the typical failure modes, the most common bond tests and two of the most important design guidelines for FRP NSM systems are introduced. In the second part, a database of bond tests composed by 431 records is presented and the accuracy of existing design guidelines is assessed with this data. Lastly, the formulations proposed by these design guidelines are recalibrated based on the experimental results in the database.

Keywords: FRP; NSM; Bond; Review

1. Introduction

The near-surface mounted technique (NSM) is one of the most effective techniques to strengthen concrete structures, mainly in bending and shear. It consists on inserting the reinforcement material in the concrete cover of the element to be strengthened. The use of fiber reinforced polymers (FRP) as reinforcing material in the context of the NSM technique has been intensively studied in the last 15 years allowing its widespread application.

The methods for application of FRP NSM systems depend on the FRP cross-section geometry. Nevertheless, the main steps are common to all FRP systems as follows: (i) execution of grooves on the face of the element to be strengthened; (ii) cleaning of grooves with compressed air or water under pressure (in the end the grooves' surfaces should be dry and without any bond-inhibiting substances); (iii) preparation of the FRP (cutting with the desired length and cleaning); (iv) preparation of the adhesive (groove filler) according to its technical specifications; (v) application of the adhesive in the grooves; (vi) insertion of the FRP into the grooves under slight pressure to force the adhesive to flow between the FRP and the groove borders. This phase requires special care in order to assure that the grooves are completely filled with adhesive. When this is not the case, the formation of voids might occur; (vii) removal of excess adhesive and groove external surface leveling.

When compared with the Externally Bonded Reinforcement (EBR) technique, NSM has the following key advantages [1-3]: (i) reduced amount of preparation work, requiring only the opening of the grooves avoiding removal of degraded surface and regularization of remaining surface; (ii) less prone to premature debonding because the bonded area is larger, allowing a more efficient use of the reinforcement material (in some cases, FRP failure can be achieved); (iii) ease in extending the reinforcement to adjacent elements; (iv) greater protection of the FRP against external aggressive agents or acts of vandalism; (v) smaller visual impact.

In terms of FRP cross-section, rectangular, square or round bars are commonly used. As the grooves have vertical and parallel sides, square and rectangular bars explore better this grooves' geometry since a more uniform adhesive thickness is achieved. Moreover, with the use of round bars, split of the groove filling cover may occur due to the existing stresses perpendicular to the FRP. In the case of square and rectangular bars this normal stress component acts mainly towards the groove lateral concrete.

Comparing square and rectangular bars, the latter maximize the ratio of surface to cross-section area, minimizing the bond stresses for the same tensile force in the FRP. Other advantage of using

rectangular bars is related with the simplicity of opening the grooves: a single saw cut is normally enough for obtaining the groove while with round/square bars two saw cuts and removal of the concrete in between are usually required. The main disadvantage of rectangular bars is the need for a deeper groove to provide the same reinforcement area.

In terms of the adhesives used to bond FRP bars to concrete, epoxy adhesives are the most common, even though some researchers have used cement mortar [4, 5]. In general, cement based adhesives have lower mechanical strength and higher curing time. On the other hand, they present better performance when subjected to high temperatures.

The most recent comprehensive review on the NSM technique was published in 2007 [6]. In order to provide a wider overview of the technique, it was not focused on the bond. Moreover, since then, a manifold of experimental works focusing on bond performance of FRP NSM systems have been developed. Hence, the scope of this work is to provide a review on the bond behavior of FRP NSM systems in concrete. This review includes, in the first part, an introduction to the typical observed failure modes, the most commonly used bond tests and two of the most important design guidelines. In the second part of this paper, a database of 431 bond tests is presented, the accuracy of the design guidelines is tested and several modifications to these guidelines' formulations are proposed.

2. FRP NSM technique

2.1. Failure modes at structural level

Considering a reinforced concrete element strengthened in bending (and/or shear) with a FRP NSM system, six failure modes combining different stress states on the three intervening materials (concrete, reinforcement steel and FRP) can occur.

Assuming firstly the failure of a single material, concrete crushing, FRP rupture or FRP debonding are possible. These failure modes should be avoided since they lead to brittle failures. Concrete crushing may occur when longitudinal steel reinforcement ratio is too high and/or concrete strength is too low; if FRP reinforcement ratio is too low and its bonded length is high enough, FRP rupture can occur; finally, if the strengthening configuration does not allow the mobilization of the FRP system's full strength, FRP debonding may occur even before steel yielding.

When the FRP NSM system is properly designed, the expected failure modes are the concrete crushing and steel yielding, steel yielding and FRP rupture or steel yielding and FRP debonding. The

internal cross-section equilibrium is achieved by the balance between concrete in compression and the contribution of both longitudinal steel and FRP in tension. Hence, the most efficient design solution will be the one which explores more efficiently the reinforcement materials (steel and FRP) thus conducting to concrete crushing after longitudinal steel yielding being the FRP safely close to failure. This leads to a ductile failure, with all materials being used up to their capacity.

The last two failure modes (steel yielding with FRP either in rupture or debonding) are the most difficult to prevent because the existing prediction models of bond strength are not robust enough yet. As a result, there is significant uncertainty regarding the definition of the critical failure mode, hindering the quality of strength predictions even for concrete crushing failures. In fact, if it was possible to predict the highest load that the FRP can attain without debonding, then it would be possible to design the FRP system not failing in tension. Then, it would also be possible to check, by the internal cross-section equilibrium, whether or not the concrete strength allows full load transfer.

In order to better understand the failure by debonding of the FRP, Figure 1 presents a general example of a reinforced concrete beam strengthened in bending with a FRP NSM system. This figure indicates the regions where the three major debonding failure modes can occur [7, 8]. End debonding is associated with the concentration of stresses near the ends of the FRP and starts from its extremity to the center of the beam, causing the failure of the strengthening system. Debonding caused by diagonal shear cracks, usually designated critical diagonal crack debonding, is associated with the development of a dominant shear crack. As soon as the crack reaches the FRP, it can propagate horizontally along the FRP NSM system towards the closest extremity, causing the failure of the strengthening system. Debonding caused by flexural cracks, commonly designated intermediate crack debonding, is in a manner similar to shear crack debonding phenomenon, but initiated by a flexural crack.

2.2. Failure modes at local level

Each one of the three debonding failure modes presented before can be in turn separated in four different local failure modes taking into account, not only the failure of the three materials involved in the FRP NSM system (concrete, FRP and adhesive) but also the existing interfaces (FRP/adhesive and adhesive/concrete). Figure 2 presents those failure modes for an example of a FRP NSM system with a rectangular bar.

To better explain these four failure modes, consider that the load is transferred from the FRP to concrete. Hence, it is expected that the first critical region where failure can take place will be the interface between FRP and adhesive. The resistance to this failure mode depends essentially on the degree of transverse confinement, bond length and adhesion mechanisms between FRP and adhesive.

Failure within the adhesive depends also on the degree of transverse confinement and on the mechanical properties of the adhesive (mainly shear resistance). Failure at the interface between adhesive and concrete depends on the same factors as the failure at the interface between FRP and adhesive, considering that the relevant adhesion mechanism is now between adhesive and concrete.

Finally, cohesive failure within the concrete depends also on the degree of transverse confinement and on the mechanical properties of concrete.

Another aspect that should be stressed is that the interfacial failure modes have a similar physical appearance (i.e. the elements will become simply unconnected), while in the case of cohesive failure modes (in adhesive or concrete) several variations can be found, e.g. crushed, spalled, splitted or in a state resulting from a combination of these types of failures.

Summarizing, FRP debonding can occur at one of the three zones indicated in Figure 1 along one of the four regions indicated in Figure 2. Although debonding can occur simultaneously in more than one zone (see Figure 1) and along more than one region (see Figure 2) in the same reinforced concrete element, at each level (structural and local) one of failure modes will be determinant.

2.3. NSM bond tests

The bond behavior of FRP NSM systems has been experimentally studied using the so-called bond tests. Several bond test configurations have been proposed for analyzing in detail the debonding phenomena introduced in section 2.1. These configurations can be grouped in direct pullout tests (DPT) and beam pullout tests (BPT). The DPT are more representative of end debonding and critical diagonal crack while BPT are recommended to study intermediate crack debonding.

DPT for FRP NSM systems were derived from the existing ones for reinforcement steel [9]. In the later, a concrete block is cast with a bar of steel in its center with a predefined bond length. The test consists on pulling the steel bar from the concrete block. The applied force and the correspondent slip (i.e., the relative displacement between the bar and the concrete block) are registered during the entire

test. This relation between force and slip allows the definition of the usually nominated bond-slip law, which is used to characterize the bond.

When DPT is used to study FRP NSM systems, the FRP is eccentrically located in the concrete block in order to be representative of NSM systems. A wide range of adaptations of the original setup has been proposed to study FRP NSM systems. Different setups lead to different stress states in concrete, which will be suitable to model different aspects of FRP NSM systems. A detailed description of the different test setups found in the literature and the corresponding critical appraisal of these is provided in section 3.

BPT for FRP NSM systems were adapted from the beam pullout tests for reinforcement steel [10]. In this case, two concrete blocks with same geometry are connected by a hinge system at the top and by a steel bar near the bottom. When the BPT is applied to FRP NSM systems, besides the use of FRP instead of steel, different bonded lengths between FRP and concrete are commonly used for each block composing the system. In one block, the FRP is fixed along its entire length, while in the other it is fixed in a smaller predefined length in order to localize the study of the debonding process.

Ideally, both types of tests should be used to fully characterize the bond behavior. In spite of that, as will be seen in the following sections, DPT are available in larger numbers due to the main advantages of this configuration in terms of practical use: DPT tests are easier, faster and less expensive than BPT ones. Moreover, the information given by the DPT is more important, since end debonding and critical diagonal crack occur for lower bond strengths.

2.4. NSM guidelines

In the past, several researchers have proposed formulations regarding the bond strength prediction of FRP NSM systems in concrete [6, 11]. The calibration of those formulations is normally limited to the reduced number of tests used, as well as by the type of failure modes observed in their experimental programs. More recently, some of the existing formulations were tested using experimental results available in the literature and some modifications were also proposed [11, 12].

In this work, the focus was given to the existing guidelines for the use and design of FRP NSM systems in concrete. At least four guidelines were identified, namely the CAN/CSA S6-06 from Canadian Standards Association [13], the ACI 4402R-08 from American Concrete Institute [7], the HB 305–2008

from Standards Australia [8] and the draft version of the new annex of EN 1992-1-1 (Eurocode 2: Part 1-1) by the TC250-SC2-WG1-TG1-N17 from the Comité Européen de Normalisation (CEN) [14].

Regarding the CAN/CSA S6-06 guideline, it was not considered in this study mainly because it does not propose a closed-form solution for the evaluation of the bond strength of FRP NSM systems. In fact, it refers that the bond strength should be obtained either by testing the FRP NSM system to be used, or it should be provided by the manufacturer.

The new annex of EN 1992-1-1 was also not considered in this study, since it is only applicable to FRP bars with rectangular cross-section (FRP strips). In addition, its formulation require some adhesive properties, such as tensile and compressive strengths, which are not often provided by the authors of the published experimental works, resulting in a marginal amount of specimens suitable to be analyzed. Additionally, the expression proposed by this guideline to estimate the bond strength depends on some coefficients which shall be provided by the manufacturer for each FRP NSM system, or adjusted by testing.

Therefore, only the remaining two guidelines were analyzed and are presented in the following paragraphs: (i) the "Guide for the Design and Construction of Externally Bonded FRP Systems for Strengthening Concrete Structures" (ACI 4402R-08) from the American Concrete Institute [7] referred in the present paper as ACI; and (ii) the "Design handbook for reinforced concrete structures retrofitted with FRP and metal plates: beams and slabs" (HB 305–2008) from Standards Australia [8], referred herein as SA. The formulation of both guidelines is based on the assumption that a certain bonded length (L_b) is required to develop the entire bond strength of the FRP NSM system, designated as development length (L_d). If $L_b \geq L_d$ the maximum bond force is achieved. Otherwise, it will be linearly reduced according to the ratio L_b / L_d.

To simplify the comparison between ACI and SA guidelines, Figure 3 presents their bond-slip laws while the following paragraphs describe each guideline's formulation. This figure also shows two idealized bond-slip models assumed as representative of the real behavior in FRP NSM systems in concrete: in general, a linear branch can be assumed for the pre-peak branch; depending on the friction degree, a horizontal plateau can exist or not in the softening phase.

2.4.1. ACI Formulation

In the ACI formulation, the key parameter is the maximum bond strength (τ_{max}) for the entire system (FRP/adhesive/concrete). If the bonded length (L_b) is greater or equal than the development length (L_d), the idealized bilinear shear stress distribution along the bond length can be approximated to a rectangular distribution. Hence, an average bond strength (τ_{avg}), constant and equal to 6.9 MPa for all FRP NSM systems, is assumed.

By imposing this average bond strength limit to the connection's maximum capacity, the L_d and the maximum pullout force installed in the FRP (F_{fmax}) can be estimated using equations (1) and (2), respectively. According to this standard if $L_b \geq L_d$ the failure will occur by FRP rupture. Otherwise it will occur by one of the four bond failure modes referred before (see Figure 2), namely failure at the interfaces FRP/adhesive or adhesive/concrete or cohesive failure at the adhesive or concrete. However, since all modes are addressed using a single expression, no indication exist about the critical failure mode.

In this formulation, F_{fmax} is predicted using only four parameters: FRP perimeter (p_f), cross-section area (A_f) and design tensile strength (f_{fd}) and the bonded length (L_b).

$$L_d = A_f f_{fd} / p_f \tau_{avg} \tag{1}$$

$$F_{f\max} = \begin{cases} A_f f_{fd} & if\ L_b \geq L_d \\ A_f f_{fd} \dfrac{L_b}{L_d} & if\ L_b < L_d \end{cases} \tag{2}$$

2.4.2. SA Formulation

The SA formulation is somehow more robust than the previous one as it was developed by solving the fundamental second order differential equation governing the bond phenomenon of FRP NSM systems assuming the theoretical bilinear bond stress slip relationship without plateau (see Figure 3). This bilinear law can be simplified to a single linear descending branch since the error associated to this simplification was found to be marginal [15]. With this strategy, the values of L_d and F_{fmax} can be estimated by using equations (3) and (4), respectively. Besides the parameters defining the bond-slip law (τ_{max} and δ_{max}), these equations include the axial stiffness of the FRP bar (EA_f) and the perimeter of the failure surface (L_{per}). SA defines that this failure perimeter is located 1 mm from the FRP bar perimeter. The SA standard also includes expressions for the estimation of the bond strength (τ_{max}) and corresponding slip

(δ_{max}). The evaluation of these entities (see equations (5) and (6)) are dependent on the concrete compressive strength (f_c) and on the ratio between the depth and the width of failure perimeter (φ_{per}).

Although SA and ACI guidelines present similar strategies for assessing F_{fmax}, there are interesting differences between them. The most relevant is that, while ACI only accounts for two types of failure modes (either be FRP rupture or an unspecified out of the four premature bond failure modes), SA accounts for three (FRP rupture, concrete cohesive failure or an unspecified premature bond failure mode out of the remaining three, i.e. cohesive at the adhesive or at the interfaces).

While in ACI guideline, the first branch of F_{fmax} equation ($L_b \geq L_d$) is associated with FRP rupture, in SA standard it is associated with concrete cohesive failure instead. SA second branch ($L_b < L_d$) is associated with the remaining three premature bond failure modes (again, not specifying which). Finally, the right-hand side of both branches introduces the FRP rupture failure mode by limiting the maximum pullout force to the tensile strength of the FRP.

The use this formulation requires the definition of the following parameters: FRP geometry (for the evaluation of L_{per} and φ_{per}), FRP design tensile strength (f_{fd}), modulus of elasticity (E_f) and cross-section area (A_f), bonded length (L_b) and concrete compressive strength (f_c).

Finally, it should be stressed that SA formulation was developed for rectangular FRP bars. However, in the scope of the present work, it was also extended to square and round FRP bars. The necessary adaptations will be detailed further.

$$L_d = \frac{\pi}{2\sqrt{\frac{\tau_{\max} L_{per}}{\delta_{\max} (EA)_f}}} \tag{3}$$

$$F_{f\max} = \begin{cases} \sqrt{\tau_{\max} \delta_{\max}} \sqrt{L_{per} (EA)_f} \leq A_f f_{fd} & if \ L_b \geq L_d \\ \sqrt{\tau_{\max} \delta_{\max}} \sqrt{L_{per} (EA)_f} \frac{L_b}{L_d} \leq A_f f_{fd} & if \ L_b < L_d \end{cases} \tag{4}$$

$$\tau_{\max} = (0.078 \varphi_{per} + 0.8) f_c^{0.6} \tag{5}$$

$$\tau_{\max} \delta_{\max} = 0.73 \varphi_{per}^{0.5} f_c^{0.67} \tag{6}$$

2.4.3. Construction details

In addition to the evaluation of the F_{fmax} and L_d, it is also necessary, from both regulatory and practical standpoints, to define a set of construction details. The guidelines presented before (ACI and SA) provide some of these construction details.

From the bibliographic survey performed (detailed in the next sections), a review on these construction details was made and is summarized in Table 1. In this table acceptable limits for the groove width (b_g), depth (d_g) and spacing (a_g), as well as edge distance (a_e) are given. It shall be stressed that the values in this table were obtained from different experimental programs, using different FRP NSM systems and test configurations.

As can be seen, in terms of groove width, only a lower limit was found in the literature. This limit aims at avoiding adhesive splitting due to the radial stresses in the FRP. However, an upper limit should also be defined in order to prevent the cohesive shear failure of the adhesive [3]. Regarding the groove depth, from the literature it is clear that the bond performance increases with the grooves' depth; however, this parameter is limited by concrete cover. A minimum value for the spacing between grooves (a_g) is proposed to avoid group effect between consecutive FRP reinforcements. Similarly, a minimum value for a_e is suggested to avoid the premature failure of the edge of the concrete element.

3. Databases of bond tests

In order to allow a deeper understanding on the bond behavior between FRP and concrete in FRP NSM systems, two databases of existing experimental programs were gathered, one for direct pullout tests (DPT) and other for beam pullout tests (BPT).

Regarding DPT, experimental results were gathered from a total of 26 documents [3-5, 19-41]. From those, 363 useful specimens were collected. For BPT, only 6 documents [4, 42-46] were found in the literature from which 68 useful specimens were selected. Table 2 presents a summary of the range of the most important parameters included in the referred databases. The following paragraphs summarize the main variables studied in the experimental programs collected, as well as the major conclusions that can be drawn by considering them all together.

Bonded length

In general, increasing the bonded length (L_b) leads to an increase in terms of the FRP maximum pullout force (F_{fmax}) and the corresponding strain (ε_{fmax}). Contrarily, the average tangential stresses in both interfaces (FRP/adhesive and adhesive/concrete) decrease due to the higher contact area between the FRP and surrounding materials and the non-uniform distribution of bond stresses along the bond length. These findings are valid both for DPT [3, 4, 20, 21, 31, 41] and BPT [4, 42, 44-47] specimens.

Regarding DPT only, since there are specimens with very small values of L_b, it was found that the average bond stresses at the interfaces increase with the increase of L_b up to a threshold (L_d), after which it decreases. The L_d value was found to be equal to $5d_f$ [24, 48] and $9.1d_f$ [32] for CFRP round bars. Taking into account that those values depend on the discrete values of L_b that were tested, a global threshold of 100 mm can be defined. For both CFRP rectangular bars [3] and GFRP round bars [35] this limit is suggested to be equal to 200 mm.

Even though the parameters that influence the definition of this limit (L_d) are not yet clearly identified, its existence has been proved experimentally. In fact, a minimum L_b is required to allow the mobilization of the entire bond-slip law. If a L_b larger than L_d is available, as the region near the loaded extremity becomes unbonded, the bond stresses migrate to the "extra" L_b. However, the maximum tangential stress value would not change since it is assumed that the local bond stress is a mechanical characteristic of the strengthening system.

FRP fiber type and external surface

The type of FRP as well as the external surface play an important role in bond response of FRP NSM systems. In identical DPT specimens and FRP NSM system configurations, it was found that F_{fmax} increases when moving from basalt to glass and from glass to carbon FRP bars [25, 27, 28, 37]. This is a consequence of the observed increasing stiffness from basalt to carbon.

As expected, smooth surfaces are more prone to failure in the FRP/adhesive interface. On the other hand, such failure modes are less sudden than the ones observed in roughened surface bars [27, 28].

Comparing FRP bars with different external surfaces it was found that F_{fmax} increases from manually roughened to sand coated to ribbed surfaces [36]. This behavior is related with the increase of the mechanical interlocking between the adhesive and the FRP surface provided by each type of external surface.

For BPT specimens it was verified that ribbed bars were more efficient than sandblasted ones [4]. This observation is in agreement with the results observed in DPT.

Groove surface

In the context of strengthening reinforced concrete structures, grooves are opened on the existing concrete cover. In spite of that, there are some studies in the literature associated with pre-molded grooves [49]. Rough grooves (as a result of opening grooves in cured concrete) behaved much better than smooth ones (associated with pre-molded grooves) since the latter are more prone to failure at adhesive/concrete interface [4].

FRP axial stiffness

For the case of DPT, F_{fmax} increases with FRP axial stiffness (EA_f) up to the value of 8000 kN, from which no further load increase was observed [25]. To confirm the existence of such limit, Figure 4a presents the relationship between EA_f and ε_{fmax}. For round FRP cross-section, ε_{fmax} decreases with EA_f (lognormal trend with R^2=0.79). In the other cases (i.e. rectangular and square bars), since the dispersion of values is low nothing can be concluded, even though the trend in rectangular bars seems to be identical to the one observed in round bars.

Similar conclusions to the ones observed in the DPT can be pointed out for the case of BPT specimens (see Figure 4b). The major differences are that: (i) no square specimens exist; (ii) the trend lines in rectangular and round FRP cross-section now are almost the same.

FRP cross-section geometry

Literature has been confirming that the FRP cross-section geometry also influences the bond performance. In fact, when the diameter (or the width for the case of rectangular cross-sections) of the FRP (d_f) increases, F_{fmax} and ε_{fmax} also increase and the tangential stress at FRP/adhesive interface ($\tau_{avg,F/A}$) decreases due to the greater contact area between the FRP bar and the adhesive [4, 5, 20].

For the case of CFRP round bars, the influence of d_f seems to be also dependent on the groove size. F_{fmax} increases with d_f if the ratio groove depth to bar diameter (d_g / d_f) is kept almost constant [31], i.e. if the groove geometry (assuming that the width is equal to the depth) also increase at the same rate. But if the groove geometry is kept equal when d_f increases, then F_{fmax} decreases [37], due to the reduction

on the adhesive thickness. As explained in section 2.4.3, there is a minimum adhesive thickness required to prevent the cohesive failure at the adhesive. In [37], the reduction on the groove size changed the failure mode from cohesive at concrete to cohesive at the adhesive.

For the case of CFRP rectangular bars, increasing the FRP bar width (b_f) increases the F_{fmax} mainly due to the larger cross-sectional area of the FRP [3, 33].

Comparing directly specimens with FRP bars with different cross-sections, it is also confirmed that rectangular bars are more efficient, in terms of exploring the FRP capacity, than round bars [45], since, as previously referred, rectangular bars explore better the surface to cross-section area ratio.

Groove's geometry

The influence of the groove's geometry was assessed by testing identical specimens where only the groove dimensions were changed. When both groove dimensions increase at the same proportion, F_{fmax} increase [31]. If the failure mode is cohesive at the adhesive then the average strength at the interface FRP/adhesive increases with groove size (keeping constant the ratio width to depth) [4]. If the failure mode is at the interface adhesive/concrete, the average strength at the interface FRP/adhesive was found to decrease in [4] and to increase in [24, 48]. When increasing separately each groove dimension, it seems that depth has positive effect on F_{fmax}, due to the increase in terms of confinement provided by surrounding concrete, while the width has negative effect [40]. This emphasizes the need for an upper limit to groove's width as referred in section 2.4.3. If the failure mode is cohesive in concrete [37] or at the interface FRP/adhesive [4], increasing the groove dimensions had no influence on F_{fmax}.

Shape Ratio

Two different shape ratios were considered in this work: one for the width, $k_b = b_g / b_f$; and other for the depth, $k_d = d_g / d_f$. In these expressions b_f and d_f are the thickness and width in quadrangular FRP bars, respectively, d_f is the diameter for round FRP bars, while b_g and d_g are groove width and depth, respectively. If both shape ratios k_b and k_d are greater than 1.5 no splitting occurred at the epoxy adhesive in [25] while splitting was observed in [27, 28]. This suggests that these geometry ratio limits are not enough to avoid of adhesive splitting. Additionally, other parameters (or relations) may be required to control the adhesive splitting, for instance making these ratios dependent on the external FRP surface.

Cover of the FRP

From the results gathered, the effect of adhesive cover of the FRP was only studied for CFRP rectangular bars. It was found that F_{fmax} and the average bond strength at the two interfaces (FRP/adhesive and adhesive/concrete) increase with the increase of the cover [5]. It was also found that, when the CFRP is inserted in deeper grooves but without cover (the adhesive only exists in the interior part of the groove and up to the outer face of the CFRP), the reduction in terms of strength and post-peak behavior of the pullout force *versus* slip relationship is small [33]. In any case, it should be kept in mind that in this case the failure mode was the same for both specimens with and without cover (cohesive within the concrete).

Concrete strength

As for the externally bonded reinforcement, concrete plays a critical role on the performance of the NSM strengthening technique. By default the maximum pullout force (F_{fmax}) increases with the concrete compressive strength (f_c) up to a threshold value [3]. This threshold value corresponds to the change of the failure mode type from cohesive within concrete to another mode. As expected, when the failure mode is not cohesive within concrete, f_c had no effect in F_{fmax} [40, 42].

For the case of specimens where failure occurred in the concrete, a reasonably constant value was obtained for the ratio between F_{fmax} and the square root of f_c, implying that the ultimate load is directly related to the tensile strength of the concrete [3].

In [31] the effect of the concrete strength on F_{fmax} seemed to be dependent of the FRP bar surface configuration and on the bonded length. Different surface configurations result in different adhesion mechanisms which, as referred in section 2.2, have a major influence in the obtained failure mode. Regarding L_b, it was found that the influence of f_c is greater in specimens with lower L_b, which is corroborated by the results presented in [45].

Bond test type

One critical aspect in the analysis of bond in NSM systems is the inexistence of a standard configuration for both direct (DPT) and beam (BPT) pullout tests. In fact, in the DPT experimental works studied, four different configurations were used to study the bond behavior in FRP NSM systems. Figure 5 summarizes those configurations which have been separated by the number of test sides (single or double-shear) and the concrete stress state during the tests (compression or tension).

In general researchers use single-shear test configuration. Variations can be found in terms of concrete block shape, which can be cubic, prismatic or even C-shaped, in spite of the prismatic being the most used. Comparing single with double-shear tests, the first ones present the following advantages: (i) simpler preparation procedures since only one face of concrete block is used; and (ii) simpler control of testing procedure and results analysis since the test region is more localized. Comparing compression and tension single-shear tests, it would be expected that F_{fmax} would be higher in compression tests, as a consequence of the confinement provided by the support conditions. However, there are results of identical specimens from compression [3] and tension [25] tests, where F_{fmax} is quite similar, even though concrete presented lower mechanical properties in the case of tension tests. The main reason that can be pointed out for this similarity is related to an unbonded length that was left between the bonded region and the top of the concrete element. This can have induced a compressive strength in the top of the concrete block, limiting the difference between compression and tension tests. In fact, the effect of leaving such unbonded length was assessed in compression tests and it was verified to achieve F_{fmax} identical to specimens where no unbonded length was left [3]. In any case, this must be verified experimentally since there are other parameters which may be influencing these conclusions.

The greater differences observed in the compression or tension pullout test setups can be found when the failure occurs within concrete. In compression tests, a concrete cohesive failure is generally observed, characterized by a concrete layer attached to the composite element (FRP/adhesive) after failure (e.g. [3]). For the case of tension tests, the concrete cohesive failure is characterized by a wedge of concrete starting from the free end of the connection to its loaded end (extremity closer to the loading point). Additionally, this wedge of concrete is limited by the location of the steel bars that reinforced the pullout specimen (e.g. [25]). Taking into account the type of debonding phenomena that DPT are intended to represent, namely, end debonding and critical diagonal crack (see Figure 1), it can be seen that tension tests are more representative than compression tests.

Unlike the case of DPT, almost all BPT tests studied used a common test configuration (*c.f.* section 2.3).

Comparing DPT and BPT databases, it is interesting to note that larger bonded lengths are used with DPT test. In fact, the BPT configuration requires larger concrete blocks to study longer bonded lengths, making BPT more expensive, as already referred in section 2.3.

Failure modes

As referred in section 2.2, there are five distinct failure modes that can occur in a pullout test, i.e. FRP rupture or one of the four premature bond failure modes (see Figure 2). However, the authors of the experimental works analyzed tend to report more than one failure modes for the same specimen. Sometimes this happens due to the occurrence of a sudden failure during the tests, hiding the possibility of observing the real failure mode. Additionally, in the case of BPT specimens, the test configuration itself could lead to erroneous identification of failure modes. In fact, the BPT are performed with test region (face where the FRP is applied) downwards, being more difficult to observe the development of the failure mechanism.

In order to have a homogeneous interpretation for the variety of failure modes that sometimes authors report, in the present work, those failure modes were grouped taking into account the most probable weakest component in the connection (concrete, FRP or interfaces). With this assumption, several different specific failure modes can be grouped under one of the five major failure modes' designations since in all of them the weak link is the same.

From all failure modes, failure of the FRP material is the simpler to recognize and is usually clearly reported by authors. Interfacial failure modes, FRP/adhesive and adhesive/concrete, are relatively simple to identify, even though sometimes they are referred associated to other failure mechanisms (e.g. adhesive splitting or concrete spalling). The strategy used in this work for those cases was to check, whenever photos of FRP and groove's surfaces after the test are provided. Interfacial failure modes will result in clean FRP surface without adhesive attached or in clean adhesive surface without concrete attached. Sometimes in the end of the test concrete or adhesive had split and those failure mechanisms are referred in addition to one of the interfacial failure modes but, after visual inspection, it was decided to classify those failures as interfacial. The shearing off of the FRP ribs, sometimes reported when round bars are used, was also classified as a failure at FRP/adhesive interface. In fact, mechanical interlocking between the adhesive and the ribs is part of the adherence mechanism in those types of FRP bars, in addition to chemical adhesion and friction between adhesive and FRP.

Cohesive failures, within concrete or adhesive, are mainly due to the normal stresses that develop together with longitudinal stresses during the pullout test. At some point, the normal stresses can reach concrete or adhesive tensile strength leading to its rupture. When there are doubts because both cohesive failures are reported, the specimen was classified according to its final appearance. If the groove remains

almost intact (the corners might be slightly damaged) failure was classified as adhesive, otherwise as concrete failure. In fact, if failure occurs in the adhesive layer, concrete would not be damaged. If damage in concrete exists, adhesive could still have been destroyed as a consequence of the explosive type of failure that characterizes both cohesive failures.

The proposed approach is consistent with the literature, for example, Soliman et al. [37] reported specimens where failure was cohesive at the concrete even though cracks in the adhesive were found after the test. Oehlers et al. [33] also found similar behavior in specimens without adhesive cover, where the reduction in the resistance due to the lack of cover is relatively small and concrete failure can be achieved. This corroborates the assumption that even if adhesive cover splitting occurs, the connection can still resist until concrete failure is reached due to the lateral confinement. Hence, adhesive splitting itself can sometimes be a consequence of other failure mechanism rather than the mechanism responsible for bond loss.

The classification approach presented above was used whenever authors report more than one failure mode. Unfortunately, in the majority of the specimens available in BPT database, the failure mode reported is a combination of several mechanisms. Hence, only for the case of DPT an overview of the failure modes can be provided, as illustrated in Figure 6. This figure shows that all the five failure modes referred before are relevant since they all can frequently occur. This highlights the complexity of this technique when compared to the externally bonded reinforcement technique where, in terms of premature bond failure, only detachment of concrete is relevant.

Additionally, it should be stressed that the evolution of the critical regions of failure suggested in section 2.2 is experimentally confirmed. It was hypothesized that, for identical specimens where only bonded length is successively increased, interfacial failure modes would be the first to appear (firstly at FRP/adhesive interface, then at adhesive/concrete), followed by one of the cohesive failure modes and the last to occur would be the FRP rupture. That trend is verified, for example, in the specimens of Seracino et al. [3] and Bilotta et al. [25] where, for identical specimens, the maximum pullout force is lower when failure at FRP/adhesive interface occurred, then when failure at adhesive/concrete interface occurred and finally the higher pullout forces are registered for specimens where concrete cohesive failure occurred. Identical trend was also found by Soliman et al. [37] where it also can be seen that in some cases FRP rupture is attained for bonded lengths higher than those that originated the cohesive failure of concrete.

4. Design formulations accuracy

The accuracy of the ACI and SA formulations was evaluated with the gathered databases. For each experimental test, the maximum pullout force was selected as the comparison variable.

All the analyses were performed using two distinct approaches: (i) data separated by the type of FRP cross-section; and, (ii) considering all the specimens together. The main purpose of this study is to assess the impact of having a single formulation for all FRP cross-sections, since the FRP NSM system behavior was found to be cross-section dependent, as shown in the previous sections.

For all the analyses performed two error metrics were calculated, namely, the mean absolute error (*MAE*) and the root mean squared error (*RMSE*). Those are defined in equations (7) and (8), respectively. In these equations, the error e_i for the i^{th} specimen of the total N, is the difference between the maximum pullout force numerical prediction ($F_{fmax,Num}$) and its experimental value ($F_{fmax,Exp}$), as illustrated in equation (9).

$$MAE = \sum_{i=1}^{N} |e_i| \Big/ N \tag{7}$$

$$RMSE = \sqrt{\sum_{i=1}^{N} e_i^2 \Big/ N} \tag{8}$$

$$e_i = \left(F_{f\,\max,Num}\right)_i - \left(F_{f\,\max,Exp}\right)_i \tag{9}$$

4.1. ACI standard

As referred in section 2.4.1, ACI formulation adopts a single value for the value of average bond strength (τ_{avg}), regardless to the type of FRP bar. In order to assess the impact of such assumption, in this section, three different analyses are presented differing on the value of τ_{avg}.

In a first analysis (A1), the value of 6.9 MPa suggested by the ACI for τ_{avg} was used. This analysis was used as reference and allowed assessing the accuracy of ACI formulation. In a second analysis (A2), a recalibration of τ_{avg} was tested. This new value was obtained by minimizing the sum of the predictions' errors. Finally, in the third analysis (A3), a new expression for τ_{avg} was proposed as function of the geometrical ratio defined in equation (10). In fact, it does not seem reasonable to have a constant value for τ_{avg}. In the present study the relation presented in equation (10) was proposed as an alternative, where parameters *a* and *b* were calibrated based on the results available in the database.

$$\tau_{avg} = a\left(\frac{A_f}{p_f L_b}\right)^b \quad (10)$$

In the case of direct pullout tests (DPT) database, the number of specimens used in all the three analyses, divided by FRP cross-section type, was: 175 rectangular, 35 square and 153 round. Figure 7 presents the results obtained in the three analyses in terms of relationship between experimental and predicted pullout force. As it can be seen in all charts, the accuracy of the predictions improved from first to second analysis and from this to the third one, confirming that τ_{avg} is cross-section dependent. This conclusion is also corroborated by the error metrics stored in Table 3, which decrease from analyses A1 to A3.

It was also interesting to find that, when all specimens are considered together, the value of 6.91 MPa for τ_{avg} was obtained in the analysis A2, which is practically the value recommended by ACI. This suggests that ACI's proposal is adequate if a single value of τ_{avg} is to be used for all geometries.

In the case of BPT database, the number of specimens used in all the three analyses, divided by FRP cross-section type, was: 33 rectangular and 35 round. Figure 8 and Table 3 present the results obtained in the three analyses using BPT database, where it can be seen that the same conclusions drawn before for DPT remain valid in BPT, i.e. from A1 to A3 analyses the results were successively better.

4.2. SA standard

As referred before, the formulation included in the SA was developed for rectangular FRP bars and assumes that the failure perimeter is located 1 mm apart from the FRP bar perimeter.

In order to assess the possibility of extending this formulation to square and round FRP bar cross-sections, two different analyses were conducted differing in terms of the location of failure perimeter. The first analysis (A1) coincides with that foreseen in SA formulation, thus the failure perimeter was assumed to be located 1 mm from the FRP bar perimeter, being the FRP located in the middle of the groove. Special care was taken to consider the different FRP cross-sections available in both databases. This failure perimeter was nominated $L_{per,f}$ since it is related with the FRP geometry.

To make the failure perimeter independent from the FRP cross-section, a second scenario was considered in which the failure perimeter was assumed to be located 1 mm from the groove perimeter. In this second analysis (A2) the failure perimeter was designated $L_{per,g}$ since it is related with the groove geometry.

After applying SA formulation with these two different failure perimeters, it was found that the second scenario (i.e. $L_{per,g}$) resulted in lower prediction errors, for both DPT and BPT databases. This conclusion is quite interesting since it allows having a single formulation for both types of tests in addition to be FRP cross-section's independent.

Having the failure perimeter location defined (i.e. $L_{per,g}$), a third analysis (A3) was then carried out. In this third analysis, the parameters of SA formulation that were obtained from experimental calibration, were recalibrated using the databases presented herein and a strategy identical to that used by SA authors [15]. This strategy consists on, based on the experimental results, calibrating the coefficients included in equations (5) and (6).

Identically to what was made earlier for DPT analyses, Figures 9 and 10 present the relationship between experimental and predicted pullout force for the three analyses with SA formulation using DPT and BPT databases, respectively, while Table 4 presents the error metrics for all the analyses with SA standard.

Since the first two analyses to choose the failure perimeter location (A1 and A2), depend on different parameters and considering that those were not always provided by the experimental works' authors, the number of specimens used in each one varies. Hence, the legend of the first two analyses also include the number of specimens used (presented in parentheses).

In the case of the third analysis (A3), the legend of each figure includes only the final recalibrated expressions. Since the failure perimeter considered is the same of A2 analysis (i.e. $L_{per,g}$), the number of specimens is also the same, thus was not repeated.

Both Figures 9 and 10 show the better performance of analysis A2 (using $L_{per,g}$) when compared with analysis A1 (using $L_{per,f}$), as referred before. Regarding the recalibration analysis (A3), it can be seen that the predictions improved when compared with analysis A2, which uses also $L_{per,g}$ but the original SA expressions as presented in equations (5) and (6). This was already expected since the number of specimens used in this work is larger than that used by SA's authors and an adjustment in the coefficients of those expressions would probably be necessary. Additionally, it can be seen that SA formulation presents better results for FRP rectangular bars than for round bars. This is related with the fact that SA formulation was derived for rectangular bars, thus not accounting for the specific bond behaviour of FRP round bars.

5. Conclusions

In this work an attempt was made to jointly analyse a large number of experimental works of pullout tests with FRP NSM systems. The following major conclusions can be drawn:

- the great majority of the experimental works' authors tend to present several failure modes since they look essentially to the final appearance of the specimens. However, as referred in this document, it would be preferable to indicate only the conditioning failure mode. Further research is necessary to define a standard method to define and describe the failure modes observed;

- regarding the definition of standard pullout tests, beam pullout tests identical to those from steel are a consensual option. Once a standard geometry is chosen, this type of test will be fully defined. In the case of direct pullout tests, further experimental work shall be carried out to choose between compression or tension single shear tests. In fact, as it was verified in this work, the final proposal of a standard direct pullout test for FRP NSM systems would be one of these two;

- the ACI and SA guidelines needed to be upgraded with new features in order to be more accurate. In this work, a proposal considering different expressions for different FRP cross-sections seemed to improve the accuracy of the proposals in ACI and SA. In fact, experimental results show that different FRP cross-sections behave differently both in terms of stress transfer and failure modes. In addition, there are failure modes which are not explicitly accounted for in these two formulations. This gap should also be bridged in the future;

- regarding SA formulation, it was verified that it can be extended to quadrangular and round bars by considering that the failure perimeter is 1 mm from the groove, rather than 1 mm from the FRP as SA establishes. However, further improvements are still necessary since the predictions for FRP rectangular bars are significantly better than those obtained for round bars;

- a common trend verified in the first analyses (A1) of both guidelines (ACI/SA) and both databases (DPT/BPT), i.e. the analyses according to each guideline, is that the amount of points below the 45 degree line in the charts is in general greater, i.e. the guidelines' predictions tend to be conservative. Contrarily, the remaining analyses tend to present a similar amount of specimens in both sides of that line. Even though this may indicate that the suggestions left in this paper are less safe than those proposed by the guidelines, those are actually more correct. In fact, considering the philosophy presented in the Eurocodes [50], a prediction model should predict the phenomenon on its average being the model's safety provided by safety factors to obtain then. Hence, no safety features should be included in the

prediction model. In this scenario, the amount of points in both sides of 45 degree line should be almost 50%;

- Finally, considering the amount of parameters which can influence the bond behavior of FRP NSM systems, it can be said that the proposal for a holistic model for predicting their strength will be very difficult to obtain. However, considering that the number of different FRP NSM systems found in the experimental works collected is quite small, it could perhaps be better to consider FRP NSM systems' certification instead of trying to certify the NSM technique itself regardless to the reinforcement system being used.

Acknowledgements

This work was supported by FEDER funds through the Operational Program for Competitiveness Factors - COMPETE and National Funds through FCT (Portuguese Foundation for Science and Technology) under the project CutInDur PTDC/ECM/112396/2009. The first author wishes also to acknowledge the Grant No. SFRH/BD/87443/2012 provided by FCT.

References

[1] EI-Hacha R, Rizkalla S. Near-Surface-Mounted Fiber-Reinforced Polymer Reinforcements for Flexural Strengthening of Concrete Structures. ACI Structural Journal. 2004;101(5):717-26.

[2] Parretti R, Nanni A. Strengthening of RC Members Using Near-Surface Mounted FRP Composites: Design Overview. Advances in Structural Engineering. 2004;7(6):469-83.

[3] Seracino R, Jones NM, Ali MSM, Page MW, Oehlers DJ. Bond Strength of Near-Surface Mounted FRP Strip-to-Concrete Joints. Journal of Composites for Construction. 2007;11(4):401-9.

[4] De Lorenzis L. Strengthening of RC structures with near surface mounted FRP rods [PhD Thesis]: University of Leece, Italy; 2002.

[5] Macedo L, Costa I, Barros J. Assessment of the influence of the adhesive properties and geometry of CFRP laminates in the bond behavior. BE2008 - Betão Estrutural 2008. Guimarães, Portugal. 2008. p. 10.

[6] De Lorenzis L, Teng JG. Near-surface mounted FRP reinforcement: An emerging technique for strengthening structures. Composites Part B: Engineering. 2007;38(2):119-43.

[7] ACI. Guide for the Design and Construction of Externally Bonded FRP Systems for Strengthening Concrete Structures. Report by ACI Committee 4402R-08. American Concrete Institute, Farmington Hills, MI, USA. 2008. p. 76.

[8] SA. Design handbook for RC structures retrofitted with FRP and metal plates: beams and slabs. HB 305 - 2008. Standards Australia GPO Box 476, Sydney, NSW 2001, Australia. 2008. p. 76.

[9] RILEM. RC 6: Bond test for reinforcement steel. 2. Pull-out test. RILEM Recommendations for the Testing and Use of Constructions Materials. 1983. p. 218 - 20.

[10] RILEM. RC 5: Bond test for reinforcement steel. 1. Beam test. RILEM Recommendations for the Testing and Use of Constructions Materials. 1982. p. 213 - 7.

[11] Lee D, Cheng L. Bond of NSM systems in concrete strengthening – Examining design issues of strength, groove detailing and bond-dependent coefficient. Construction and Building Materials. 2013;47(0):1512-22.

[12] Bilotta A, Ceroni F, Nigro E, Pecce M. Strain assessment for the design of NSM FRP systems for the strengthening of RC members. Construction and Building Materials. 2014;69(0):143-58.

[13] CSA. Canadian Highway Bridge Design Code. CAN/CSA S6-06, Canadian Standards Association, Canada. 2006. p. 734.

[14] CEN. Strengthening with FRP. Draft version TC250-SC2-WG1-TG1-N17. Comité Européen de Normalisation, Bruxeles. 58.

[15] Seracino R, Saifulnaz MR, Oehlers DJ. Generic Debonding Resistance of EB and NSM Plate-to-Concrete Joints. Journal of Composites for Construction. 2007;11(1):62-70.

[16] Hassan T, Rizkalla S. Bond mechanism of near-surface-mounted fiber-reinforced polymer bars for flexural strengthening of concrete structures. ACI Structural Journal. 2004;101(6):830–9.

[17] Blaschko M. Bond behaviour of CFRP strips glued into slits. FRPRCS-6. Singapore. 2003. p. 205–14.

[18] Kang J-Y, Park Y-H, Park J-S, You Y-J, Jung W-T. Analytical evaluation of RC beams strengthened with near surface mounted CFRP laminates. FRPRCS-7. Kansas City, Missouri, USA. 2005. p. 16.

[19] Rashid R, Oehlers DJ, Seracino R. IC Debonding of FRP NSM and EB Retrofitted Concrete: Plate and Cover Interaction Tests. Journal of Composites for Construction. 2008;12(2):160-7.

[20] Thorenfeldt E. Bond capacity of CFRP strips glued to concrete in sawn slits. FRPRCS-8. Patras, Greece. 2007. p. 10.

[21] Teng JG, De Lorenzis L, Wang B, Li R, Wong TN, Lam L. Debonding Failures of RC Beams Strengthened with Near Surface Mounted CFRP Strips. Journal of Composites for Construction. 2006;10(2):92-105.

[22] Mitchell PA. Freeze-thaw and sustained load durability of near surface mounted FRP strengthened concrete [MSc Thesis]: Queen's University, Canada; 2010.

[23] De Lorenzis L, Lundgren K, Rizzo A. Anchorage length of near-surface mounted fiber-reinforced polymer bars for concrete strengthening — Experimental investigation and numerical modeling. ACI Structural Journal. 2004;101(2):269-78.

[24] Novidis DG, Pantazopoulou SJ. Bond Tests of Short NSM-FRP and Steel Bar Anchorages. Journal of Composites for Construction. 2008;12(3):323-33.

[25] Bilotta A, Ceroni F, Di Ludovico M, Nigro E, Pecce M, Manfredi G. Bond efficiency of EBR and NSM FRP systems for strengthening concrete members. Journal of Composites for Construction. 2011;15(5):757-72.

[26] Bilotta A, Ceroni F, Di Ludovico M, Nigro E, Pecce M, Manfredi G. Experimental bond test on concrete members strengthened with NSM FRP systems: influence of groove dimensions and surface treatment. CICE 2012. Rome, Italy. 2012. p. 8.

[27] Palmieri A, Matthys S, Barros J, Costa I, Bilotta A, Nigro E, et al. Bond of NSM FRP strengthened concrete: round robin test initiative. CICE 2012. Rome, Italy. 2012. p. 8.

[28] Palmieri A, Matthys S, Taerwe L. Double bond shear tests on NSM FRP strengthened members. CICE 2012. Rome, Italy. 2012. p. 8.

[29] Barros J, Costa I. Bond Tests on Near Surface Reinforcement Strengthening for Concrete Structures. Report of the Round Robin Tests 22 carried out by EN-CORE Project at University of Minho. University of Minho, Guimarães, Portugal. 2010. p. 53.

[30] Yun Y, Wu Y-F, Tang WC. Performance of FRP bonding systems under fatigue loading. Engineering Structures. 2008;30(11):3129-40.

[31] Kalupahana W. Anchorage and Bond Behaviour of Near Surface Mounted Fibre Reinforced Polymer Bars [PhD Thesis]: University of Bath, United Kingdom; 2009.

[32] Yan X, Miller B, Nanni A, Bakis C. Characterization of CFRP Rods Used as Near Surface Mounted Reinforcement. 8th International conference on structural faults and repair, Engineering Technics Press. Edinburgh, Scotland. 1999. p. 12.

[33] Oehlers DJ, Haskett M, Wu C, Seracino R. Embedding NSM FRP plates for improved IC debonding resistance. Journal of Composites for Construction. 2008;12(6):635-42.

[34] Shield C, French C, Milde E. The effect of adhesive type on the bond of NSM tape to concrete. FRPRCS7. Kansas City, Missouri, USA. 2005. p. 355-72.

[35] Wang B, Teng JG, Lorenzis LD, Zhou L-M, Ou J, Jin W, et al. Strain monitoring of RC members strengthened with smart NSM FRP bars. Construction and Building Materials. 2009;23(4):1698-711.

[36] Lee D, Hui J, Cheng L. Bond characteristics of NSM reinforcement in concrete due to adhesive type and surface configuration. CICE 2012. Rome, Italy. 2012. p. 8.

[37] Soliman SM, El-Salakawy E, Benmokrane B. Bond performance of Near-Surface-Mounted FRP bars. Journal of Composites for Construction. 2011;15(1):103-11.

[38] Lundqvist J. Numerical analysis of concrete elements strengthened with carbon fiber reinforced polymers [PhD Thesis]: Luleå University of Technology, Sweden; 2007.

[39] Seo S-Y, Feo L, Hui D. Bond strength of near surface-mounted FRP plate for retrofit of concrete structures. Composite Structures. 2013;95(0):719-27.

[40] Al-Mahmoud F, Castel A, François R, Tourneur C. Anchorage and tension-stiffening effect between near-surface-mounted CFRP rods and concrete. Cement and Concrete Composites. 2011;33(2):346-52.

[41] Capozucca R. Analysis of bond-slip effects in RC beams strengthened with NSM CFRP rods. Composite Structures. 2013;102(0):110-23.

[42] Sena-Cruz JM. Strengthening of concrete structures with near-surface mounted CFRP laminate strips [PhD Thesis]: University of Minho, Portugal; 2004.

[43] Kotynia R. Bond between FRP and concrete in reinforced concrete beams strengthened with near surface mounted and externally bonded reinforcement. Construction and Building Materials. 2012;32(0):41-54.

[44] Martin T, Cleland D, Robinson D, Taylor SE. Experimental study of bond stress for near surface mounted basalt fibre reinforced polymer strips on concrete. Bond in Concrete 2012. Brescia, Italy. 2012. p. 991-8.

[45] Merdas A, Fiorio B, Chikh NE. Bond behavior of carbon laminate strips and rods into concrete by pullout-bending tests. Bond in Concrete 2012. Brescia, Italy. 2012. p. 1087-92.

[46] Novidis DG, Pantazopoulou SJ. Beam Pull Out Tests of NSM – FRP and Steel Bars in Concrete. Fourth International Conference on FRP Composites in Civil Engineering (CICE2008). Zurich, Switzerland. 2008. p. 7.

[47] Lundqvist J, Nordin H, Taljsten B, Olofsson T. Numerical analysis of concrete beams strengthened with CFRP - a study of anchorage lengths. International Symposium on Bond Behaviour of FRP in Structures (BBFS2005). Hong Kong, China. 2005. p. 247-54.

[48] Novidis D, Pantazopoulou SJ, Tentolouris E. Experimental study of bond of NSM-FRP reinforcement. Construction and Building Materials. 2007;21(8):1760-70.

[49] De Lorenzis L, Rizzo A, La Tegola A. A modified pull-out test for bond of near-surface mounted FRP rods in concrete. Composites Part B: Engineering. 2002;33(8):589-603.

[50] CEN. Eurocode - Basis of structural design. EN 1990:2002 E. Comité Européen de Normalisation, Bruxeles. 2002. p. 87.

Table Captions

Table 1 – Recommended construction details for FRP NSM systems

Table 2 – Summary of the main variables included in the gathered databases.

Table 3 – Error metrics obtained in all the analyses with ACI standard.

Table 4 – Error metrics obtained in all the analyses with SA standard.

Table 1 – Recommended construction details for FRP NSM systems.

<table>
<tr><th>FRP bar cross-section</th><th>Groove width (b_g)</th><th>Groove depth (d_g)</th><th>Groove spacing (a_g)</th><th>Edge distance (a_e)</th></tr>
<tr><td rowspan="2">Round</td><td>$\geq 1.5d_f$ [4]</td><td>$\geq 2.0d_f$ [4]</td><td rowspan="2">$\geq 2.0d_f$ [16]</td><td rowspan="2">$\geq 4.0d_f$ [16]</td></tr>
<tr><td colspan="2">$\geq 1.5d_f$ [7]</td></tr>
<tr><td rowspan="2">Quadrangular</td><td rowspan="2">$\geq b_f + 3.0$ [17]
$\geq 3.0b_f$ [7]</td><td rowspan="2">$\geq d_f + 3.0$ [17]
$\geq 1.5d_f$ [7]</td><td>≥ 53.0 [19]
$> 2.0d_g$ [7]</td><td>$\max\left\{\begin{matrix}30.0\\ \text{aggregate size}\end{matrix}\right\}$ [17]
$\geq 3.5d_f$ [19]
$> 4.0d_g$ [7]</td></tr>
<tr><td colspan="2">≥ 40.0 [18]</td></tr>
</table>

Notes: All units are in millimeters; d_f – FRP round bar diameter or quadrangular bar width; b_f – FRP quadrangular bar width.

Table 2 – Summary of the main variables included in the gathered databases.

Parameter		DPT	BPT	Variable		DPT	BPT
Number of tests by FRP fiber type	C	308	54	Number of tests by FRP cross-section type	REC	175	33
	G	28	6		SQU	35	0
	B	27	8		ROU	153	35
L_b [mm]		[30-510]	[40-305]	E_f [GPa]		[37-273]	[34-171]
f_c [MPa]		[18.4-65.7]	[26.7-73.5]	f_{fu} [MPa]		[512-3100]	[773-2833]
b_f [mm]		[1.2-10.0]	[1.4-2.5]	A_f [mm^2]		[12-201]	[13-143]
d_f [mm]		[6-40]	[8-20]	$(EA)_f$ [kN]		[1301-27300]	[429-20268]
F_{fmax} [kN]		[8.8-205.1]	[2.9-61.9]	ε_{fmax} [‰]		[0.7-27.9]	[1.1-27.8]

Legend: Type of FRP fiber: C – Carbon, G – Glass, B – Basalt; L_b – bond length; f_c – concrete compressive strength; b_f – FRP thickness; d_f – FRP width or diameter; F_{fmax} – FRP maximum pullout force; Type of FRP cross-section: REC – Rectangular, SQU – Square, ROU – Round; E_f – FRP modulus of elasticity; f_{fu} – FRP tensile strength; A_f – FRP cross-section area; $(EA)_f$ – FRP axial stiffness; ε_{fmax} – strain in the FRP corresponding to F_{fmax}.

Table 3 – Error metrics obtained in all the analyses with ACI standard.

Database	FRP cross-section	Rectangular		Square		Round		All	
	Analysis	MAE [kN]	RMSE [kN]	MAE [kN]	RMSE [kN]	MAE [kN]	RMSE [kN]	MAE [kN]	RMSE [kN]
DPT	A1	16.53	21.81	19.69	21.73	11.83	15.34	14.85	19.34
	A2	16.01	24.10	19.42	23.13	11.25	14.78	14.85	19.34
	A3	13.19	18.17	13.03	16.01	9.89	13.21	14.43	19.12
BPT	A1	8.25	9.21	-	-	12.92	16.66	10.65	13.56
	A2	7.08	8.39	-	-	11.53	14.23	10.61	12.98
	A3	7.29	9.03	-	-	9.57	12.67	9.76	12.32

Table 4 – Error metrics obtained in all the analyses with SA standard.

Database	FRP cross-section	Rectangular		Square		Round		All	
	Analysis	MAE [kN]	RMSE [kN]	MAE [kN]	RMSE [kN]	MAE [kN]	RMSE [kN]	MAE [kN]	RMSE [kN]
DPT	A1	13.61	18.62	23.53	27.36	14.06	16.26	14.95	18.87
	A2	10.71	15.14	20.04	23.84	10.11	11.99	11.56	15.16
	A3	9.73	14.13	16.85	20.75	7.42	9.70	10.59	14.14
BPT	A1	5.61	6.94	-	-	11.13	12.39	8.45	10.12
	A2	5.24	6.71	-	-	9.00	10.57	7.18	8.90
	A3	4.81	5.84	-	-	7.14	9.51	6.23	7.68

Figure Captions

Figure 1 – Principal debonding failure modes in a beam strengthened in flexure with a FRP NSM system.

Figure 2 – Four possible failure modes associated with debonding phenomenon.

Figure 3 – Bond-slip laws for FRP NSM systems.

Figure 4 – Influence of EA_f in ε_{fmax}: (a) DPT database; (b) BPT database.

Figure 5 – Summary of DPT configurations used in the works collected: single-shear compression (a) and tension (b) test; double-shear compression (c) and tension (d) test.

Figure 6 – Summary of failure modes for the specimens in DPT database. NOTE: C – concrete cohesive failure; F – FRP rupture; A – adhesive cohesive failure; F/A – failure at FRP/adhesive interface; A/C – failure at adhesive/concrete interface; NR – not reported.

Figure 7 – Results for the analyses with ACI standard (DPT database): (a) all 363 specimens; (b) 175 rectangular specimens only; (c) 35 square specimens only; (d) 153 round specimens only.

Figure 8 – Results for the analyses with ACI standard (BPT database): (a) all 68 specimens; (b) 33 rectangular specimens only; (c) 35 round specimens only.

Figure 9 – Results for the analyses with SA standard (DPT database): (a) all specimens; (b) rectangular specimens only; (c) square specimens only; (d) round specimens only.

Figure 10 – Results for the analyses with SA standard (BPT database): (a) all specimens; (b) rectangular specimens only; (c) round specimens only.

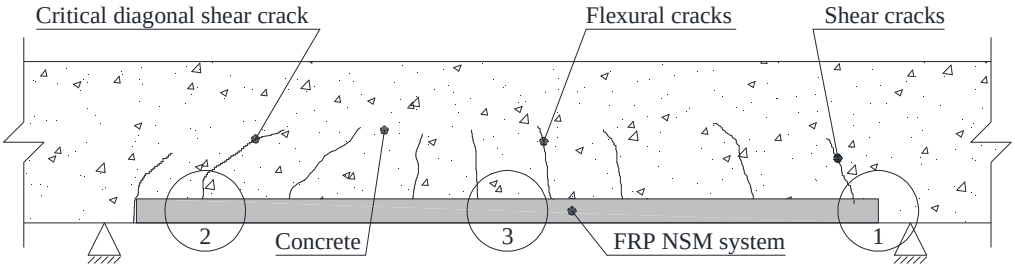

1 – End debonding; 2 – Debonding caused by diagonal shear cracks; 3 – Debonding caused by flexural cracks

Figure 1 – Principal debonding failure modes in a beam strengthened in flexure with a FRP NSM system.

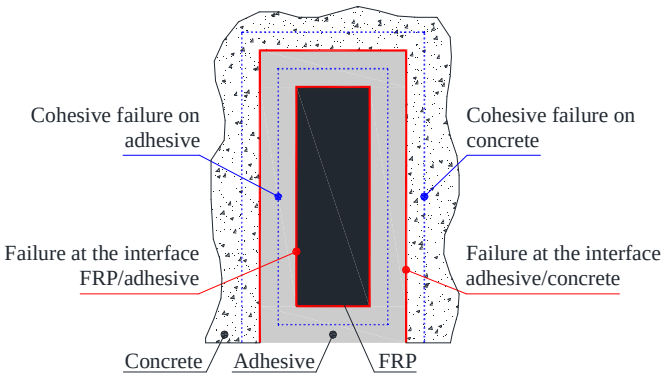

Figure 2 – Four possible failure modes associated with debonding phenomenon.

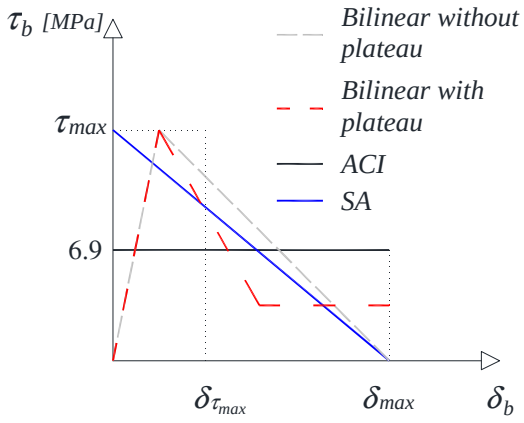

Figure 3 – Bond-slip laws for FRP NSM systems.

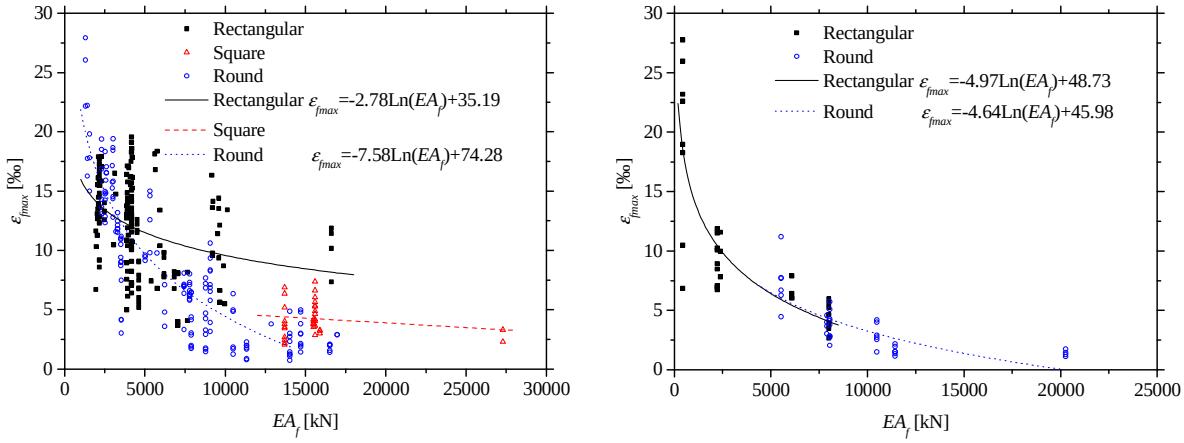

(a) (b)

Figure 4 – Influence of EA_f in ε_{fmax}: (a) DPT database; (b) BPT database.

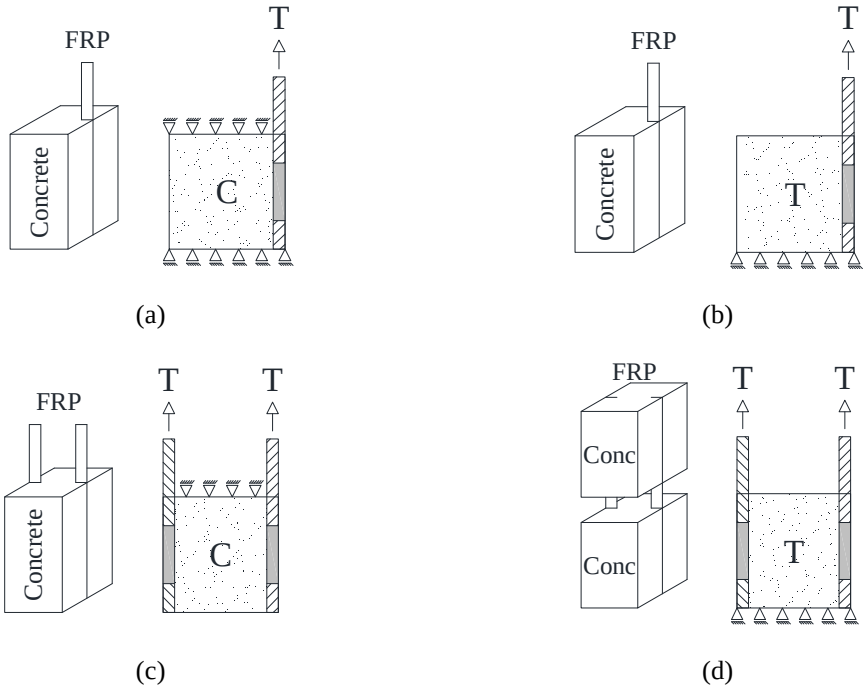

Figure 5 – Summary of DPT configurations used in the works collected: single-shear compression (a) and tension (b) test; double-shear compression (c) and tension (d) test. NOTE: C – compression; T – tension.

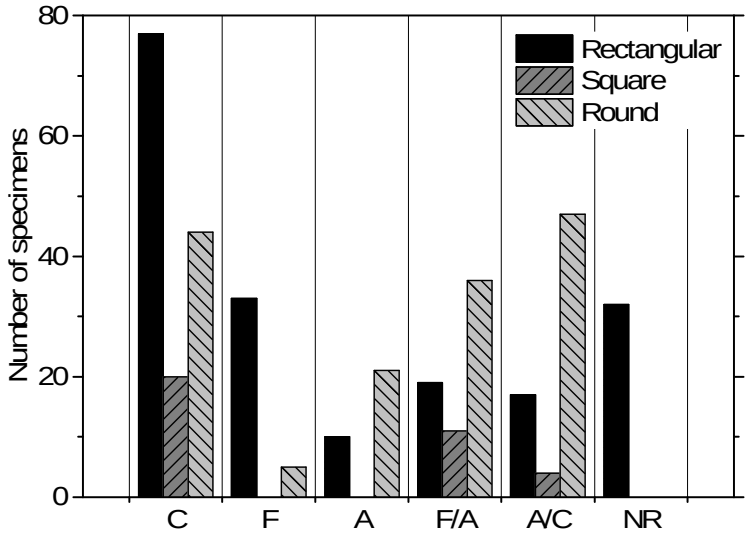

Figure 6 – Summary of failure modes for the specimens in DPT database. NOTE: C – concrete cohesive failure; F – FRP rupture; A – adhesive cohesive failure; F/A – failure at FRP/adhesive interface; A/C – failure at adhesive/concrete interface; NR – not reported.

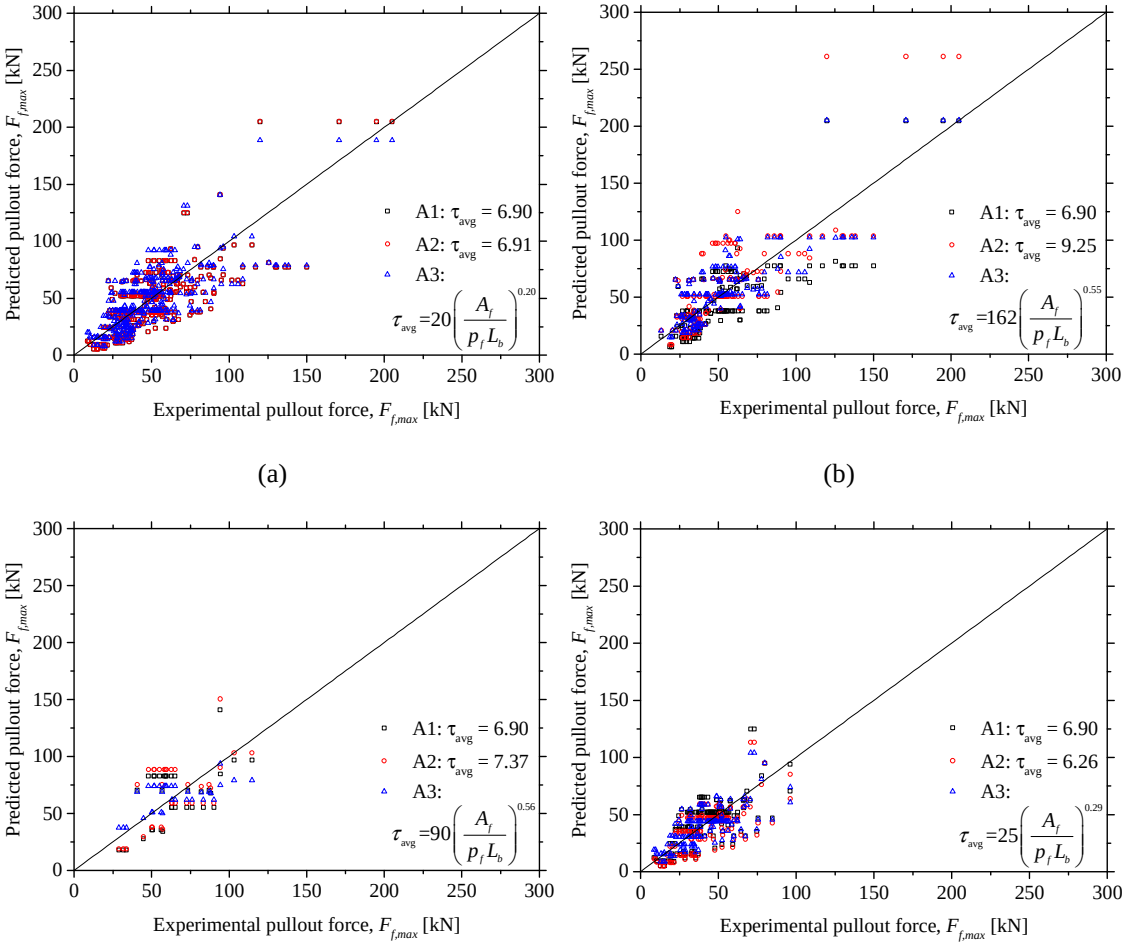

Figure 7 – Results for the analyses with ACI standard (DPT database): (a) all 363 specimens; (b) 175 rectangular specimens only; (c) 35 square specimens only; (d) 153 round specimens only. (Note: τ_{avg} in MPa; A_f in mm^2; p_f and L_b in mm)

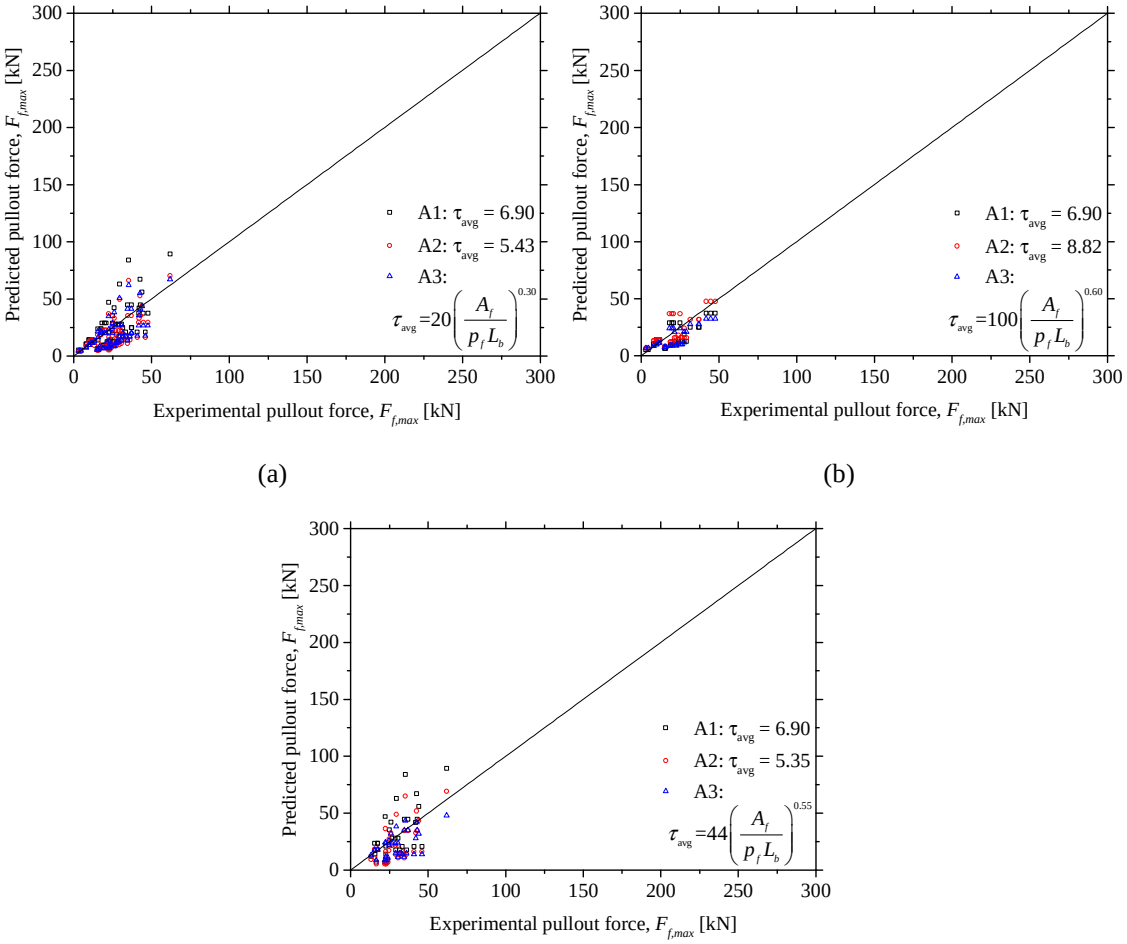

Figure 8 – Results for the analyses with ACI standard (BPT database): (a) all 68 specimens; (b) 33 rectangular specimens only; (c) 35 round specimens only. (Note: τ_{avg} in MPa; A_f in mm^2; p_f and L_b in mm)

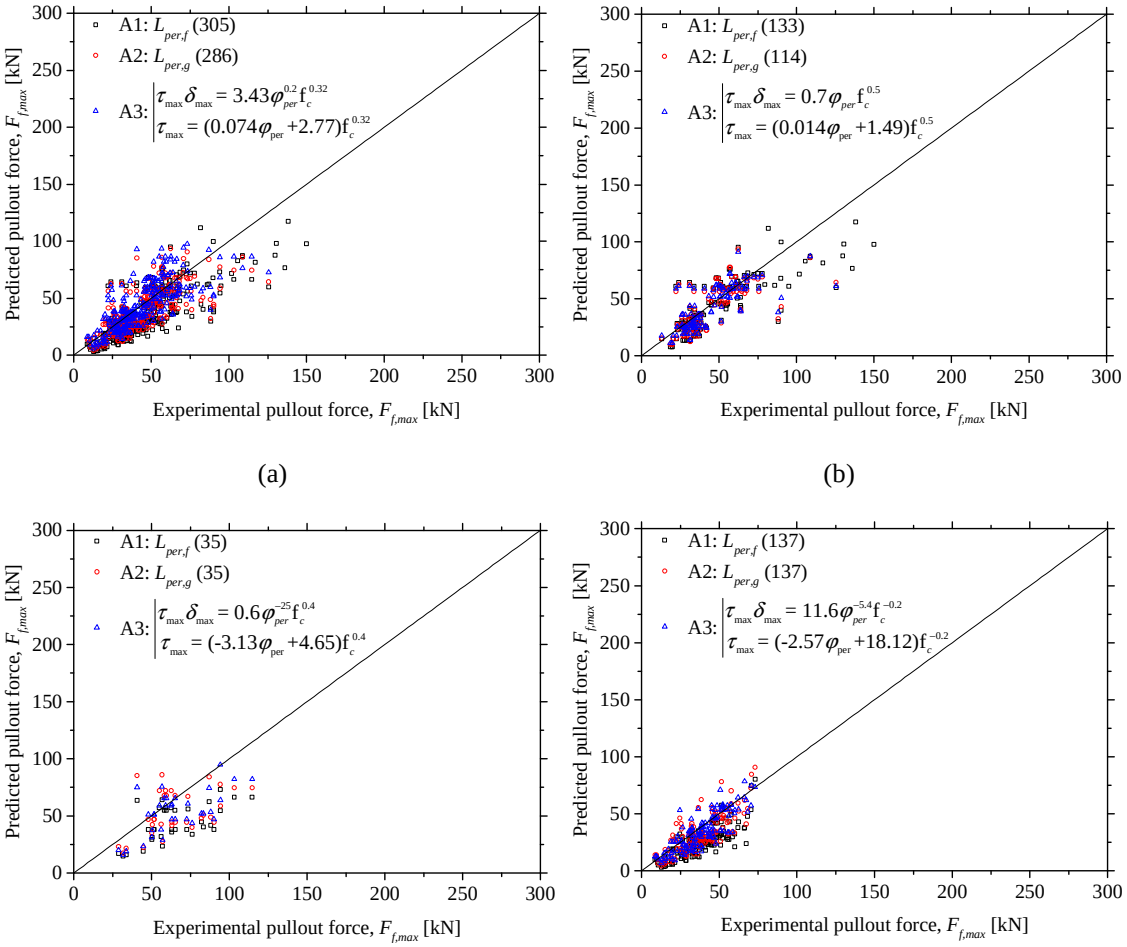

Figure 9 – Results for the analyses with SA standard (DPT database): (a) all specimens; (b) rectangular specimens only; (c) square specimens only; (d) round specimens only.

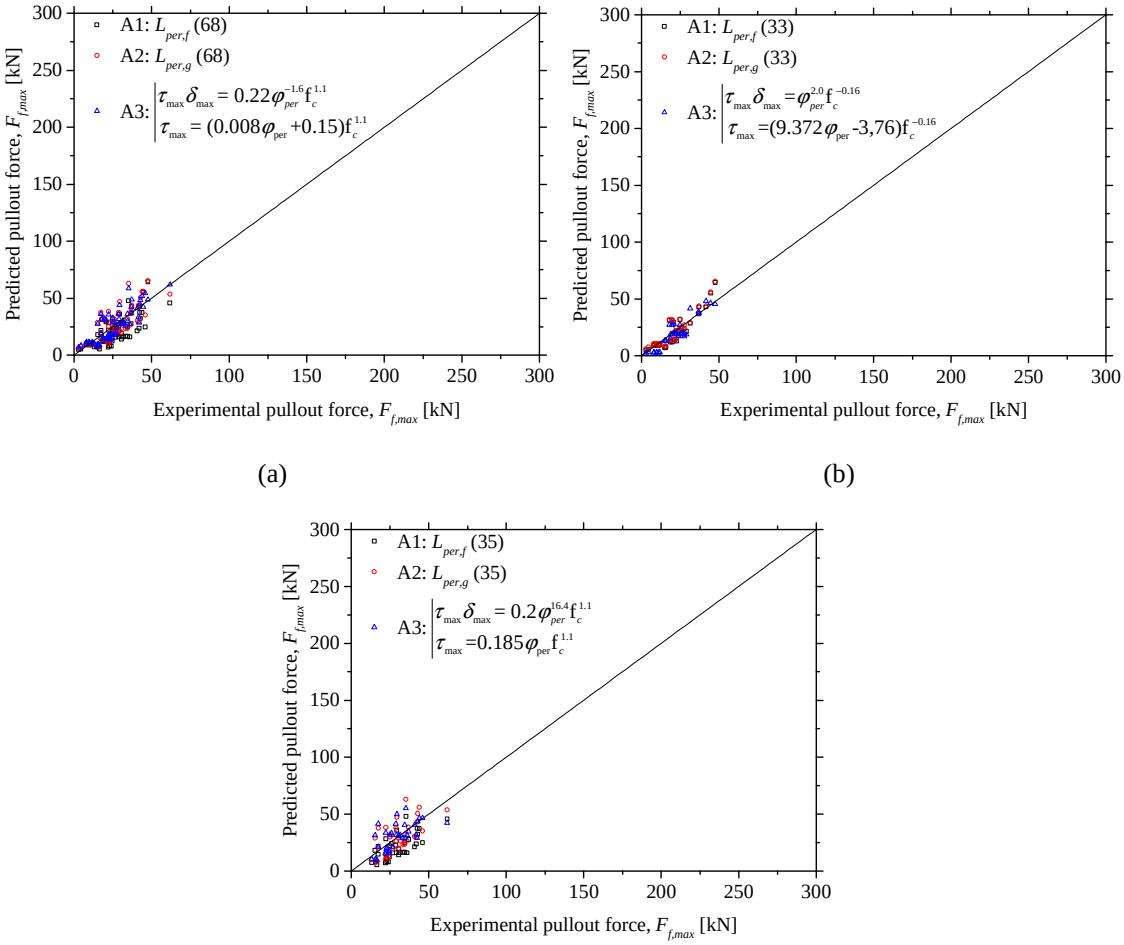

Figure 10 – Results for the analyses with SA standard (BPT database): (a) all specimens; (b) rectangular specimens only; (c) round specimens only.

Notation

The following acronyms /symbols are used in this paper:

Acronyms	
ACI	American Concrete Institute guideline
BPT	beam pullout tests
DPT	direct pullout tests
FRP	fiber reinforced polymer
NSM	near-surface mounted technique
SA	Standards Australia guideline

Symbols	
δ_{max}	maximum bond slip
ε_{fmax}	strain at F_{fmax}
φ_{per}	failure perimeter ratio
τ_{avg}	average bond strength
$\tau_{avg,F/A}$	average tangential stress at F/A
τ_{max}	maximum bond strength
A_f	FRP cross-section area
b_f	FRP thickness
b_g	groove width
d_f	FRP width or diameter in quadrangular or round bars, respectively
d_g	groove depth
E_f	FRP modulus of elasticity
f_c	concrete compression strength
F_{fmax}	maximum pullout force installed in the FRP
f_{fd}	FRP design tensile strength
f_{fu}	FRP tensile strength
k_b	groove to FRP width ratio
k_d	groove to FRP depth ratio
L_b	bonded length
L_d	development length
L_{per}	SA failure plane perimeter
p_f	FRP perimeter